Final Report of Research Project
Of
National Science Council

Intrseasonal Variation in the Velocity Field of the Northern South China Sea

By
T.Y. Tang
(唐存勇)

Institute of Oceanography
National Taiwan University
Taipei, Taiwan, R.O.C.

Research Project No：92-2611-M-002-008

Dec. 2004

1. 簡介

在計畫書中承諾以海洋數值模式配合實測海流資料，探討由呂宋海峽入侵的黑潮、南海環流、風等參數之間的交互作用，對北南海流場之季節內變動的影響；執行結果尚好，雖模式尚未建立完整，唯由分析海流流場資料獲得一些成果，並撰寫二篇論文：一為”Intra-seasonal variation in the velocity field of the northeastern South China Sea”，目前已送至 Continental Shelf Research II 審查，二位審查者建議接受但需要一定程度修改。另一篇文章名為”Energy and Characteristics of Nonlinear Internal Waves in South China Sea”已送至 Geophysical Research Letter 審查中。

第 2 章將二篇論文陳列做為此計畫的成果，第 3 章將討論結果的缺失，及未來可能進一步研究之方向。

2. 結果

Intra-seasonal variation in the velocity field of the northeastern South China Sea

Chau-Ron Wu[1], T. Y. Tang[2,*], S. F. Lin[2,3], Y. J. Yang[4], and W.-D. Liang[4]

[1]*Department of Earth Sciences, National Taiwan Normal University, Taipei, Taiwan, ROC*

[2]*Institute of Oceanography, National Taiwan University, Taipei, Taiwan, ROC*

[3]*Energy & Resources Laboratories, Industrial Technology Research Institute, Hsinchu, Taiwan, ROC*

[4]*Department of Marine Science, Chinese Naval Academy, Kaohsiung, Taiwan, ROC*

[*]***Corresponding author. Institute of Oceanography, National Taiwan University, P.O. Box 23-13, Taipei, 106, Taiwan, ROC, Tel: +886-2-23626097; Fax: +886-2-23698526; Email address: tyt@ccms.ntu.edu.tw***

Submitted to

Continental Shelf Research II

July 2004

Abstract

Two subsurface Acoustic Doppler Current Profilers (ADCP) were deployed at the northeastern South China Sea to study circulation structure in the area as well as the path and process of Kuroshio intrusion. The 48-hour low-pass filtered data reveal significant intra-seasonal variations in the velocity field. The current pattern alternates between clockwise and counterclockwise even within a single month. Local wind forcing dominated by monsoon winds fails to address the phenomena and variations. The present study suggests that wind stress curl forcing is the dominant process controlling the circulation picture in the area. While a stronger wind stress curl appeared and developed off southern tip of Taiwan, it will provide negative vorticity to the intruded current and form an anticyclonic eddy. The stronger current is always going along with the stronger wind stress curl. On the other hand, while the curl in the area looses or decays, the intruded current becomes weakened and forms a cyclonic eddy. The agreement between wind stress curl and the velocity field suggests that changes in the wind stress curl contribute to the intra-seasonal variations in the northeastern South China Sea.

Introduction

The circulation structure in the northeastern South China Sea is extremely complicated. In addition to the location with a complicated topography and seasonal reversal monsoon, the regions might be interacted between currents from both northern South China Sea and Taiwan Strait. Furthermore, it is well known that the Kruoshio front might reach the sea southwest of Taiwan and influence the shelf break circulation [*Fan and Yu*, 1981]. All of these factors induce varieties of contributions and alter the current structures in the regions. Especially the intrusion current from Kuroshio front, it might be the most important component and be the major theme in the area.

The Pacific western boundary current, the Kuroshio, flows northward and bypasses east of Luzon and Taiwan [*Nitani*, 1972]. Similar to the Loop Current in the Gulf of Mexico, the Kuroshio water has also been reported to intrude the Luzon Strait where plays a deep gap in the western boundary [*Nitani*, 1972; *Shaw*, 1991]. Since the Luzon Strait is the only deep passage of the South China Sea, the intrusion of water from Kuroshio is important to the salt budget in the basin. Seasonal variations of Kuroshio intrusion have been reported extensively in a wealth of existing literature [e. g. *Wyrtki*, 1961; *Nitani*, 1972; *Shaw*, 1991]. However, the conclusion of seasonal intrusion is challenged by several recent observations. For example, both moored current data and ship-board ADCP data evidenced that the westward trend of Kuroshio intrusion is persisted all the year round [*Liang et al*., 2003; *Tang et al*., 2003].

Furthermore, although the intrusion of waters from the Kuroshio to the northeastern South China Sea has been studied for several decades, the path and process of Kuroshio intrusion in the region remained discrepancies among oceanographers. For example, based on hydrographic data, *Wang and Chern* [1987] inferred an anticyclonic (clockwise) eddy occupied the area at the onset of the northeast monsoon. Also based on hydrographic data in May and August 1986, on the other hand, *Shaw* [1989] suggested that the intrusion current was probably part of a cyclonic (counterclockwise) circulation in the northern South China Sea. Anticyclonic or cyclonic circulation is of importance to the distribution of the water masses in the region. A correct description of circulation pattern is essential to future dynamic studies of the intrusion process.

In this study, current and hydrographic data from two mooring stations were examined to study the circulation pattern in the region. The direct observations in the velocity field are capable of determining the distribution of the Kuroshio intrusion water and inferring the path of intrusion. The results show that significant intra-seasonal variations in the velocity field. The current pattern alternates between clockwise and counterclockwise. Wind stress curls were also calculated from the blended QSCAT/NCEP (NASA Quick Scatterometer/National Centers for Environmental Prediction) wind stress fields at a resolution of 0.5° x 0.5° [*Milliff et al*., 1999] to examine the driving mechanism of the local current.

Mooring data

Two sets of subsurface moorings (named St. W and St. E) were deployed in the west and east of the shelf break northeast of the South China Sea, respectively. Figure 1 shows the mooring locations and the surrounding bathymetry. Each set of mooring includes an upward-looking, 150 *kHz*, self-contained Acoustic Doppler Current Profiler (ADCP) mounted on a 45” diameter spherical syntactic foam buoy and a SEACAT Conductivity-Temperature-Depth (CTD) mounted 5 *m* beneath the ADCP. The water depths at St. W and St. E are 1014 *m* and 968 *m*, respectively. Table 1 lists the locations and local water depths for each mooring, the depths of instruments, the duration of deployments, and the vertical range of current profile measured by the ADCP. The bin length of ADCP was set as 8 *m*. The hourly current velocity was recorded averaged over 240 pings for board-band ADCP. The standard deviations of measurement velocity were 1.2 $cm\ s^{-1}$. The obtained current velocity of ADCP was corrected for vertical excursion and sound speed by the CTD data. The data were also adjusted for local magnetic deviation. Finally, the vertical profile of current velocity was linearly interpolated and resampled at 10 *m* intervals. The time series of current velocity discussed in the following sections were low-pass filtered to remove the fluctuations for frequencies higher than 0.5 cycles per day.

Results and discussion

Low-pass filtered velocity

Figure 2 shows the eastward (U) and northward (V) components of 48-hour low-pass filtered current velocity at St. W. In general U component is stronger than V component and the currents decrease but keep the direction with depth. Both U and V components show significant intra-seasonal variations. By November 2000, U component is weak and alternates directions between westward and eastward. The current enhances and turns eastward in December, reaching its maximum strength in the end of December. Just in the beginning of January, the eastward current decreases suddenly and reverses thereafter. Until March 2001, a repeat behavior takes place when eastward flow appears in the middle of March and reaches its maximum in the end of the month, turning westward suddenly afterward. Similar pattern but leading around half month is presented in the V component. In the beginning of both December 2000 and March 2001, the V component turns southward after it accelerated northward.

Similar to Figure 2, Figure 3 shows U and V components of low-pass filtered velocity at location St. E. Significant intra-seasonal variations are also evidenced at St. E. Graphically, U component is generally weak except in October, November 2000 and February 2001 when stronger currents with speed more than 50 $cm\ s^{-1}$ occur and all of them flow eastward. Two periods of weak westward currents present in January and middle March 2001. Frequently reversal currents are shown in v component. Prior to middle of December, currents flow southward mostly, turning northward thereafter. Stronger southward currents show again in the middle of February, reaching its maximum speed of 100 $cm\ s^{-1}$ on March 1, 2001. The current turns northward in the middle of March and persists into April. Furthermore, the intra-seasonal variation at St. E seems to agree well with that at St. W, indicating that St. E and St. W are related to each other somehow. To emphasize this, the stick plots of depth average at St. W (20-130 *m*) and St. E (20-180 *m*) are shown together in Figure 4. Similar intra-seasonal reversals of currents between St. W and St. E come to the first sight. However, it seems that changes in St. E generally lead those in St. W around 10~15 days. The phenomenon deserves to further verify and will be examined in detail later in this section.

In Figure 4, northward flow prevails at St. W and southeastward flow exists at St. E prior to the middle of December 2000. The feature infers that this region is dominated by a conceptual clockwise circulation pattern. Currents at St. W reverse southwestward and meanwhile currents at St. E turn either northwestward or northeastward during the period from middle December to middle February. The reversal phenomena suggest that current pattern alters from clockwise circulation to counterclockwise in the study region. Clockwise circulation dominates again during the period from middle February to middle March. Note that the currents are always stronger during clockwise circulation. After March, weak counterclockwise circulation plays the finale. Furthermore, as mentioned in the introduction section, currents perform an anticyclone or a cyclone might directly influence the geographic distribution of the water masses in the region. Without a correct description of circulation pattern, it is not possible to identify the water masses and to verify the intrusion process.

Water masses and circulation pattern

To describe the distribution of various water masses and the path of Kuroshio intrusion, the mooring CTD data at both St. W and St. E were plotted in Figure 5. Also join with velocity vectors to separate different episodes of clockwise and counterclockwise circulation. In the figure, the red color represents circulation pattern is clockwise while the blue represents there is counterclockwise circulation. Temperature and salinity of St. W and St. E were measured at depth of around 160 *m* and 205 *m*, respectively. Although the absolute values of CTD data are probably problematic, the relative value can still be applied to identify where the water masses come from. Since not only temperature but salinity of St. E are generally lower than those of St. W, the measured depth at St. E is deeper could not account for the phenomena singly. Rather, there must be colder and fresher water entering and mixing with the local water around regions of St. E. Based on long-term mooring observations around sea southwest of Taiwan, mean current always flows southeastward during winter [*Chern*, 1982]. With mixing cold and fresh coastal water from Taiwan Strait, it makes sense that temperature and salinity at St. E should be lower than those at St. W.

Furthermore, concerning the temporal variability in each station, both stations show that temperature is higher whenever clockwise circulation dominates in the region. The temperature difference is more distinct at St. W where is far away from influence of colder coastal water (Figure 5). The higher values of temperature were presented during two periods in December 2000 and in March 2001. The results are reasonable and can be explained by water movement. Currents generally intensify while clockwise circulation performs as mentioned earlier so that stronger intrusion current brings in warmer water from Kuroshio front and then increases water temperature at St. W. On the other hand, during counterclockwise circulation episode (e.g. in the middle of January), the current is weak and flows westward continuously along its northern boundary in Taiwan Strait. By gradually mixing with cold front from Taiwan Strait, the water temperature decreases.

To further study alternation of circulation pattern and relation between St. W and St. E, we rotated the current velocity to its principal axis. The principal axis of St. W is 45° clockwise-rotated Cartesian (northeastern-southwestern) and St. E is 135° clockwise-rotated Cartesian (southeastern-northwestern). Figures 6a and 6b show time series of principal axis depth-average current velocity at St. W and St. E, respectively. Graphically, both St. W and St. E evidence two significant peaks. However, the timing is not consistent with each other. Two peaks at St. W are during the periods December and March while at St. E are from middle November to middle December and from middle February to middle March. The results demonstrate that St. E leads St. W and an interval of 315-hour might properly describe time lag of St. W. In Figure 6c, St. E with time lag of 315 hours is overlapped to St. W. Peak-to peak comparison indicates that the variations of St. W and those in time lag of St. E are frequently in phase, suggesting St. E leads St. W by 10~15 days indeed. The trend is always valid whatever during episode of clockwise or counterclockwise circulation. The fact that St. E leads St. W during clockwise episode is probably against intuitive. Therefore, not merely a single anticyclone structure might be inferred and be expected.

Mechanism

What causes the intra-seasonal variation in the area deserves to further investigate. Intuitively, currents in the area, especially those near surface currents, should be driven by the strong monsoon during winter when northeasterly winds prevail. However, there is almost no correlation between the current and local wind forcing from weather station at Tung-Chi Island (figure not shown). Based on model simulations in the South China Sea, *Wu et al*. [1998] suggested that the formation of a gyre, whatever anticyclonic or cyclonic, is essential determined by the wind stress curl. *Shaw et al*. [1999] also found that the first two empirical orthogonal functions (EOF) modes of the wind stress curl agree well with those in the corresponding altimeter sea level modes, further supporting the wind stress curl forcing scenario. However, it is not clear whether the wind stress curl is also important to meso-scale circulation as in the present study. Since the scale is quite small in the present study, high-resolution winds are indeed in need. We adopted 6-hourly maps of 10 *m* zonal and meridional wind components at a resolution of 0.5° x 0.5°, which is derived from a space and time blend of QSCAT-DIRTH satellite scatterometer observations and NCEP analyses [*Milliff et al*., 1999]. The blended data set is one of the most up-to-date high-resolution data of ocean surface winds in the present time.

In this section, wind stress curls are calculated from the blended wind stress fields. Figure 7 shows the monthly mean of the wind stress curl during the six-month period. The days in February and March 2001 have been slightly adjusted to fit the intra-seasonal variation in the velocity field. Main features in the intra-seasonal variation of the wind stress curl are captured in the sequence of plots from (a)-(f). In October 1999 (Figure 7a), a dipole structure with positive value to the north appeared in the region. Note that the south portion is what we should be more concern about since its position approaches the Kuroshio intrusion. Off southern tip of Taiwan, the large and negative curl extends southwestward in October that marks the onset of the winter monsoon. The pattern persists well into November, gradually increasing its strength in December. In the following month, the southern curl weakens (Figure 7d). The curl increases again and reaches its maximum strength during the period from February 10 to March 10 (Figure 7e) and decays afterwards (Figure 7f). The variations of the southern curl are corresponding to those shown in the velocity field and the curl is capable of explaining the intra-seasonal variations in the velocity field. While the southern curl appeared and developed in the position, the intruded current from Kuroshio would form anticyclonic eddies clockwise because the curl provides negative vorticities to the current. Note that the strongest southern curl is confined and limited near St. E. Therefore, a tight and stronger anticyclone might occur in close vicinity of St. E merely. The loosed clockwise vortexes might shed away from St. E while the corresponding Reynolds number is large enough. The large value of curl also explains the reason why the current is accelerated during clockwise circulation dominated episode as mentioned earlier. For example, the strongest southward current at St. E with maximum speed of 100 $cm\ s^{-1}$ shown on March 1, 2001 is well corresponding to the strongest southern curl in Figure 7e. On the other hand, while the southern curl weakens or looses (Figure 7d, 7f), the intruded current overwhelms the curl and continues westward along the shelf break, forming a weak cyclonic (counterclockwise) eddy. Weaker currents in these two counterclockwise episodes are also noted in the previous section.

Summary and Conclusions

Although the East Asian monsoons dominate, an intra-seasonal instead of seasonal variation in the velocity field has been found in the region. The agreement between wind stress curl and velocity fields suggests that the wind stress curl could be the main driving force to trigger the intra-seasonal variations. The intensity of wind stress curl off southern tip of Taiwan could determine whether clockwise or counterclockwise circulation pattern performs in the region. While the southern curl enhanced, the intruded current strengthens by getting large vorticity from the curl and forms an anticyclonic eddy afterwards. The mooring velocity data indeed evidence that currents during clockwise circulation are much stronger than those during counterclockwise. Temperature is also higher while clockwise since the stronger intrusion current will bring in Kuroshio warmer water and increase local water temperature.

Acknowledgements

We would like to thank Mr. Y. C. Tsai for processing the mooring data. This research was supported by the National Science Council, Taiwan, ROC, under grants NSC 89-2611-M-002-031-OP2 (TYT), NSC 91-2611-M-003-004 (CRW), and NSC 90-2611-M-012-001-OP2 (YJY).

References

Chern, C. S., Current and wave measurement in the vicinity of Hsien-Da-Kang and Tung-Kang (continued), *Special Pub. 39*, Inst. of Oceanogr., Natl. Taiwan Univ., Taiwan, 1982.

Fan, K. -L., and C.-Y. Yu, A study of water masses in the seas of south most Taiwan, *Acta Oceanogr. Taiwan.*, **12**, 94-111, 1981.

Liang, W.-D., T. Y. Tang, Y. J. Yang, M. T. Ko, and W.-S. Chuang, Upper-ocean current around Taiwan, *Deep-Sea Res. II*, **50**, 1085-1105, 2003.

Milliff, R. F., W.G. Large, J. Morzel, G. Danabasoglu, and T. M. Chin, Ocean general circulation model sensitivity to forcing from scatterometer winds, *J. Geophys. Res.*, **104**, 11337-11358, 1999.

Nitani H., Beginning of the Kuroshio, in *Kuroshio*, pp. 129-163, Univ. of Wash. Press, Seattle, Wash., 1972.

Shaw, P.-T., The intrusion of water masses into the sea southwest of Taiwan, *J. Geophys. Res*., **94**, 18213-18226, 1989.

Shaw, P.-T., S.-Y. Chao, and L.-L. Fu, Sea surface height variations in the South China Sea from satellite altimetry, *Oceanol. Acta*, **22**, 1-17, 1999.

Tang, T. Y., W.-D. Liang, Y. J. Yang, and W.-S. Chuang, Kuroshio intrusion in the Luzon

Strait, *J. Phys. Oceanogr.*, submitted, 2003.

Wu, C.-R., P.-T. Shaw, and S.-Y. Chao, Seasonal and interannual variations in the velocity field of the South China Sea, *J. Oceanogr.*, **54**, 361-372, 1998.

Wang, J. and C. S. Chern, The warm-core eddy in the northern South China Sea, Preliminary observations on the warm-core eddy, *Acta Oceanogr. Taiwan.*, **18**, 92-103, 1987.

Wyrtki, K., Physical oceanography of the southeast Asian waters, Scientific Results of Marine Investigation of the South China Sea and the Gulf of Thailand, *NAGA Report Vol. 2*, 195 pp., Scripps Institution of Oceanography, La Jolla, California, 1961.

TABLE 1. Mooring locations; water, ADCP and CTD depths; durations; and data distribution depths (interval of 10 *m*) at St. W and St. E, respectively.

Station	Longitude	Latitude	Water Depth	ADCP Depth	CTD Depth	Duration	Measurement Range
St. W	118° 44’E	22°N	1014 *m*	160 *m*	165 *m*	2000/10/13~ 2001/04/18	20~130 *m*
St. E	120° 10’E	22°N	968 *m*	202 *m*	207 *m*	2000/10/04~ 2001/04/18	20~180 *m*

Figure Captions

Figure 1. The study area with locations of mooring stations (squares) and Tung-Chi Island (asterisk). The current distribution at 30 m is adopted from *Liang et al*. [2003].

Figure 2. Vertical sections of 48-hr low-pass current velocity observed at St. W. Contour interval is 10 $cm\ s^{-1}$.

Figure 3. Same as Figure 2 except at St. E.

Figure 4. Stick plots of the depth-averaged current velocity at St. W and St. E, respectively.

Figure 5. T-S diagram at St. W and St. E. Velocity vectors are also presented to separate different episodes of clockwise (red) and counterclockwise (blue) circulation.

Figure 6. Time series of principal axis depth-average current velocity at St. W and St. E, respectively. St. E with time lag of 315 hours is overlapped to St. W shown in the bottom panel as well.

Figure 7. Monthly mean of the wind stress curl during the six-month period. Contour interval is $0.1 \times 10^{-7}\ N\ m^{-3}$. Regions of negative curls are shaded.

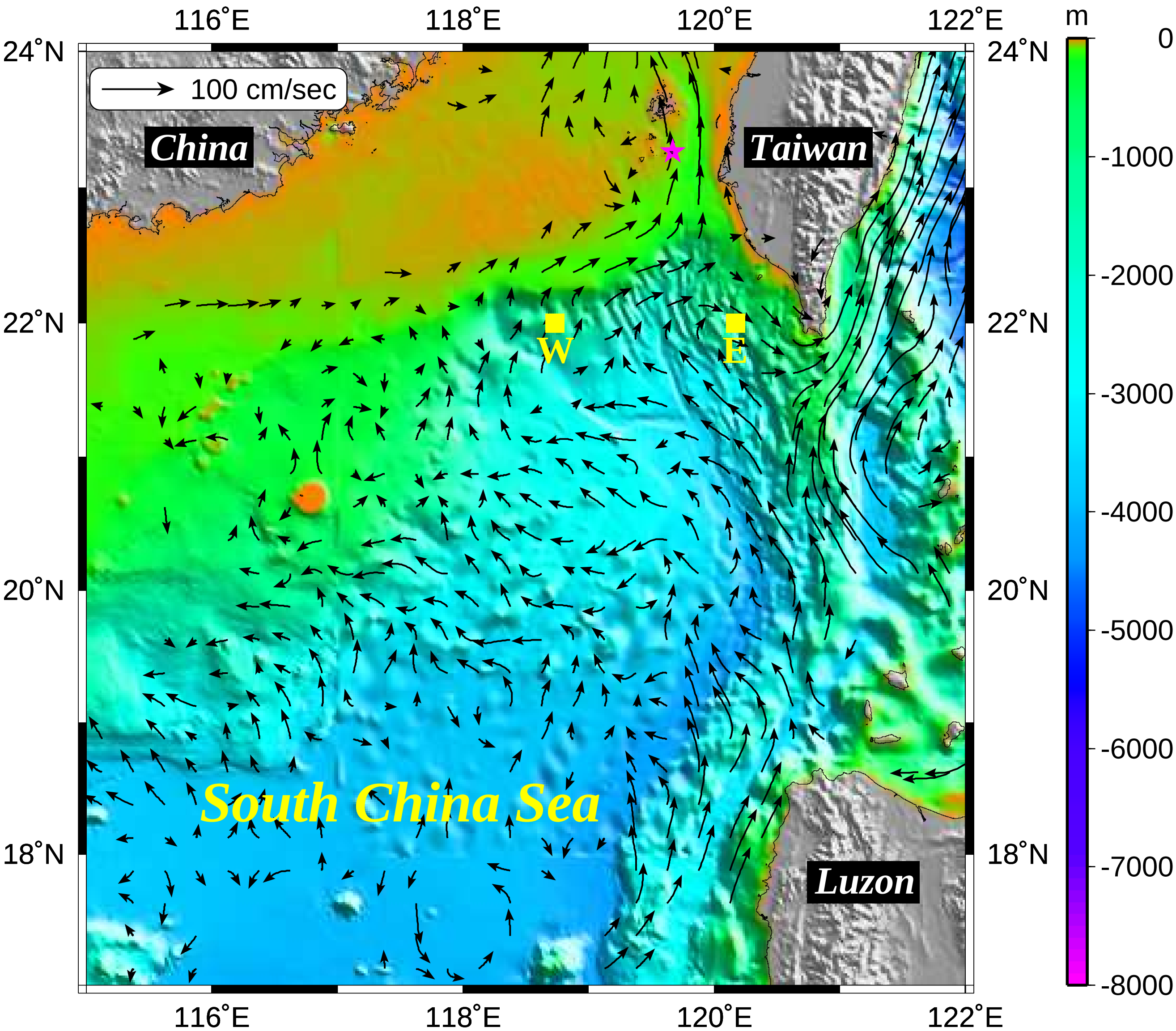

116°E
118°E
120°E
122°E
24°N
22°N
20°N
18°N
100 cm/sec
China
Taiwan
Luzon
South China Sea
W
E
m
0
-1000
-2000
-3000
-4000
-5000
-6000
-7000
-8000

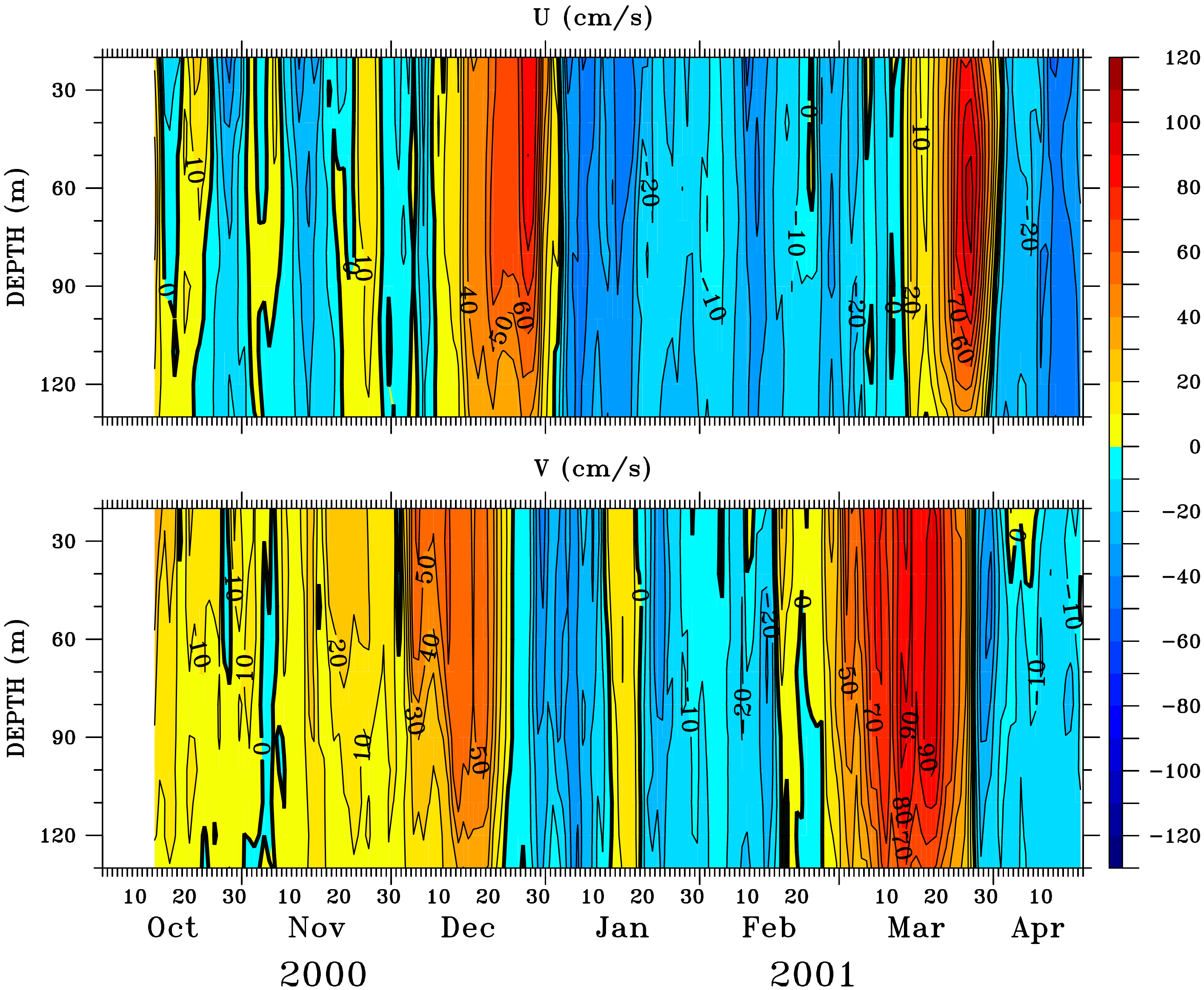

U (cm/s)
V (cm/s)
DEPTH (m)
30
60
90
120
10
20
30
Oct
Nov
Dec
Jan
Feb
Mar
Apr
2000
2001
120
100
80
60
40
20
0
−20
−40
−60
−80
−100
−120

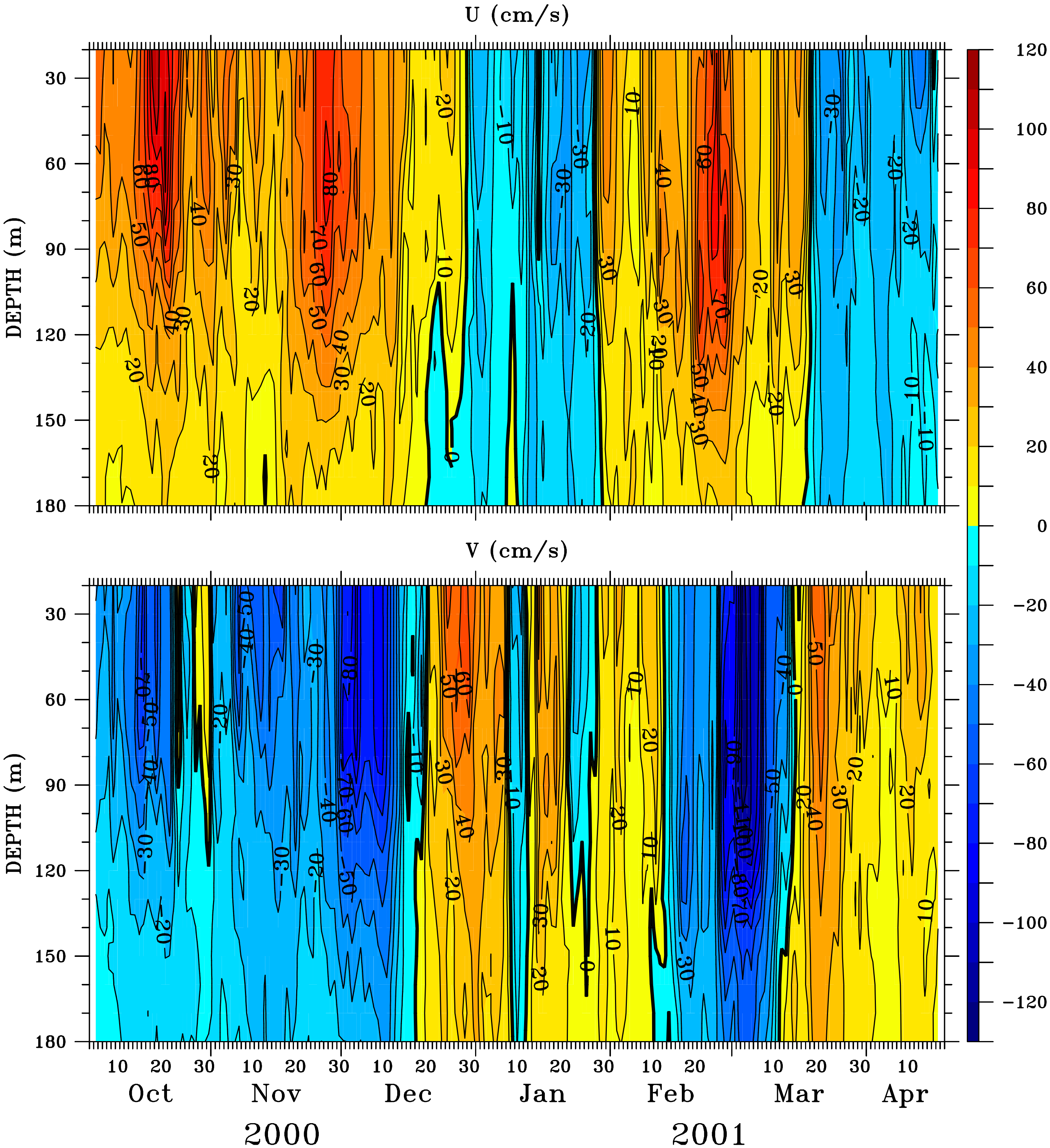
U (cm/s)
V (cm/s)
DEPTH (m)
30
60
90
120
150
180
10 20 30 10 20 30 10 20 30 10 20 30 10 20 10 20 30 10
Oct Nov Dec Jan Feb Mar Apr
2000
2001
120
100
80
60
40
20
0
−20
−40
−60
−80
−100
−120

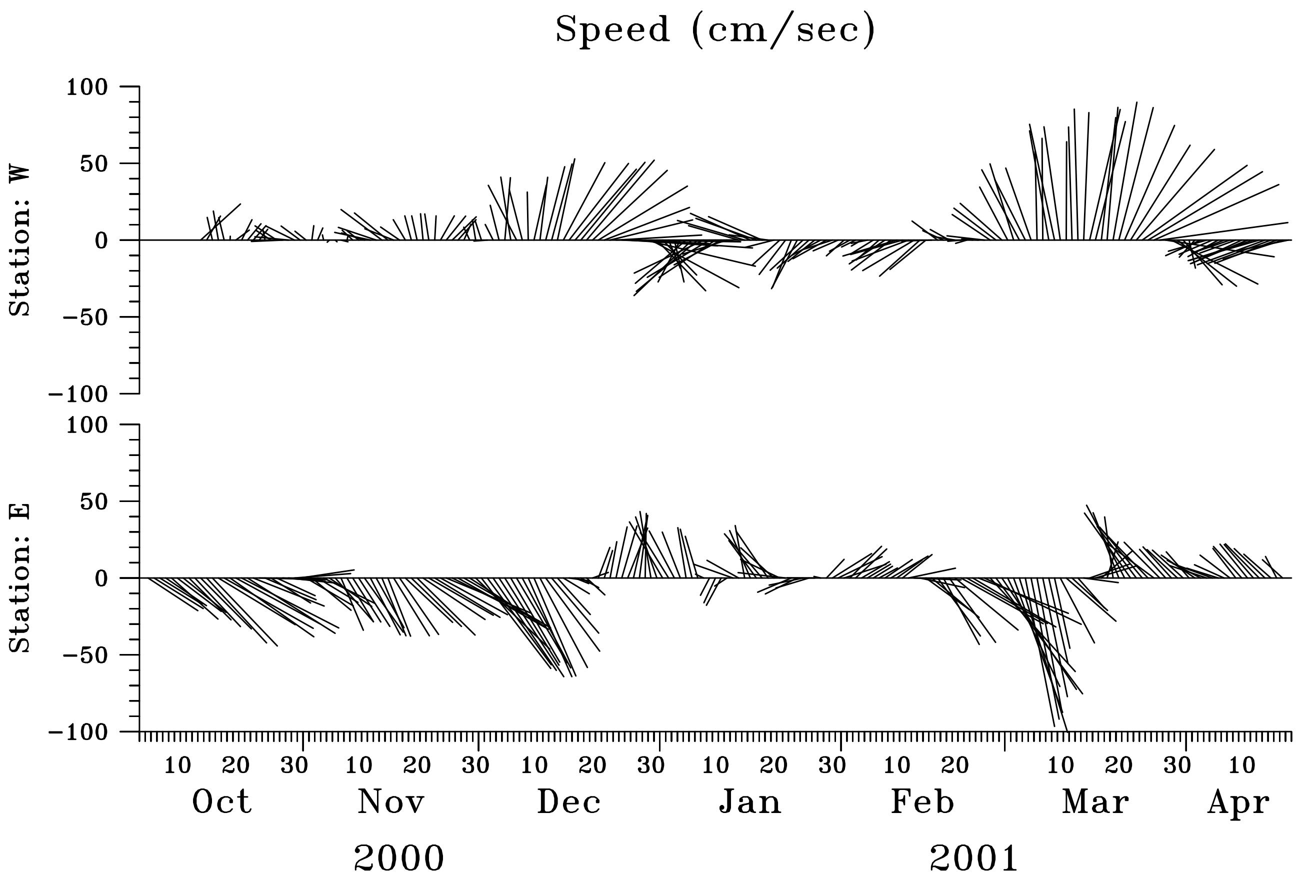

Speed (cm/sec)
Station: W
Station: E
100
50
0
−50
−100
10 20 30 10 20 30 10 20 30 10 20 30 10 20 10 20 30 10
Oct
Nov
Dec
Jan
Feb
Mar
Apr
2000
2001

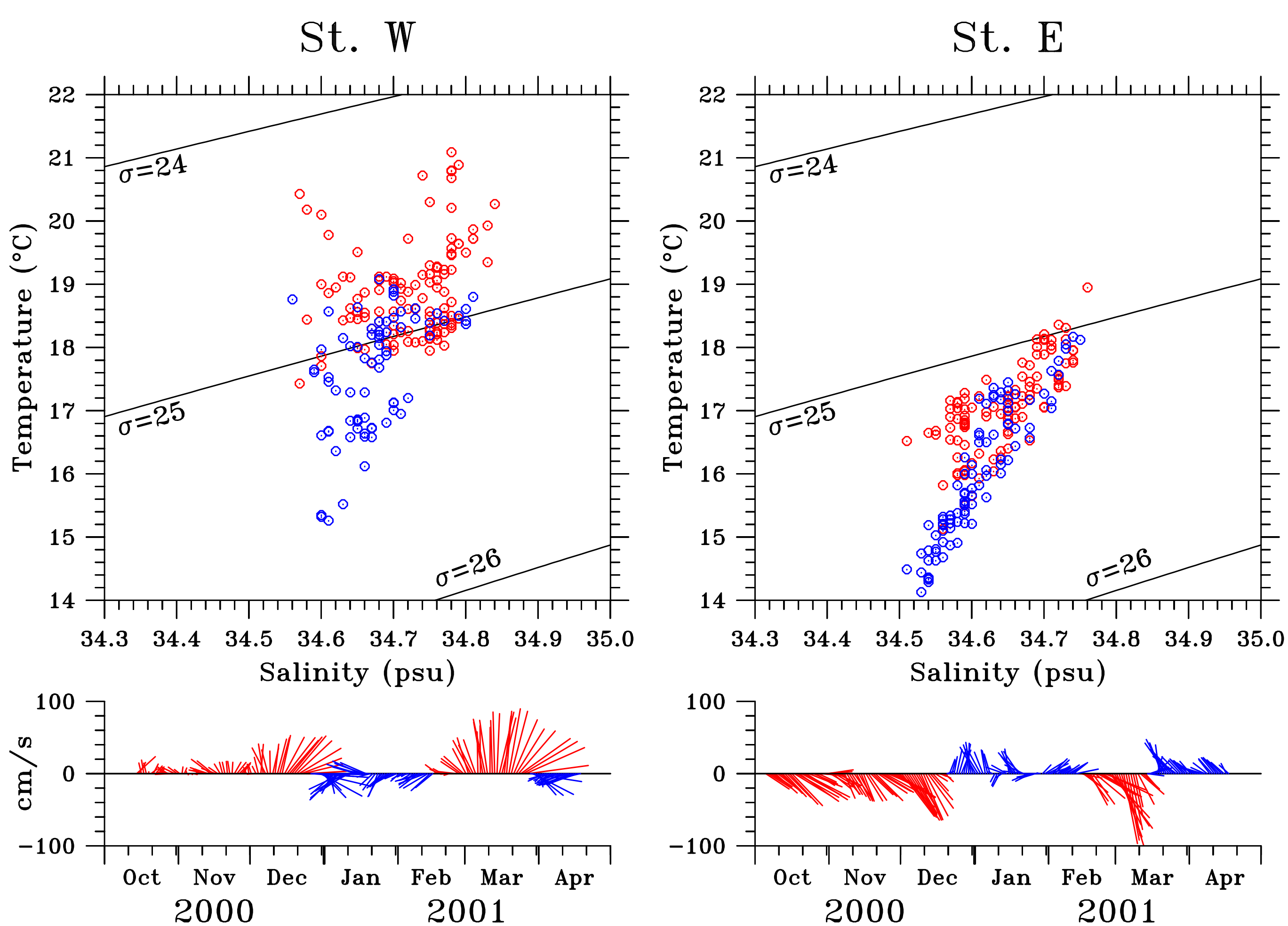
St. W
St. E
Temperature (°C)
Salinity (psu)
σ=24
σ=25
σ=26
cm/s
Oct
Nov
Dec
Jan
Feb
Mar
Apr
2000
2001

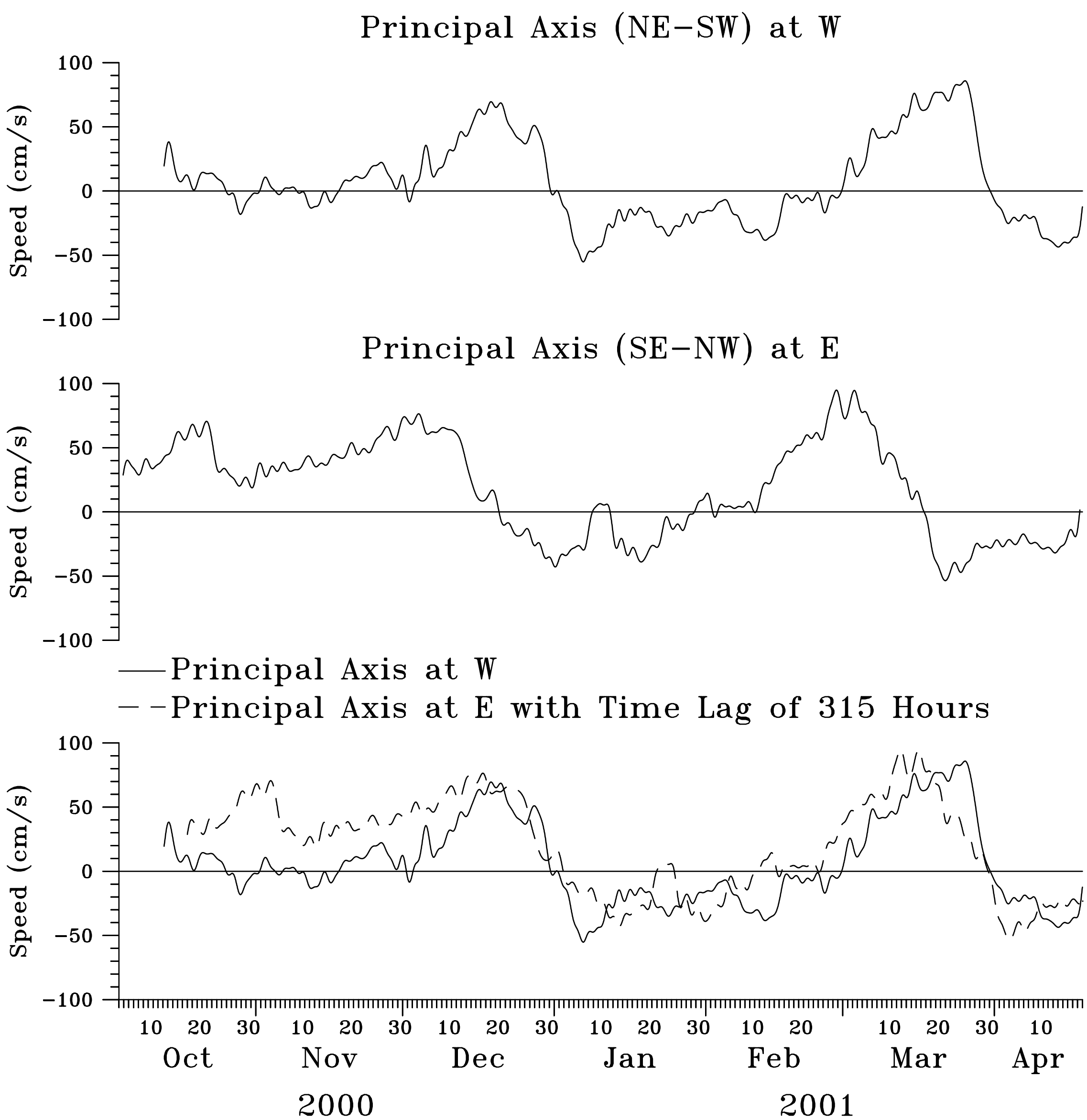
Principal Axis (NE−SW) at W
Principal Axis (SE−NW) at E
Principal Axis at W
Principal Axis at E with Time Lag of 315 Hours
Speed (cm/s)
100
50
0
−50
−100
10 20 30 10 20 30 10 20 30 10 20 30 10 20 10 20 30 10
Oct Nov Dec Jan Feb Mar Apr
2000
2001

Wind Stress Curl (× 10^{-7} N m^{-3})

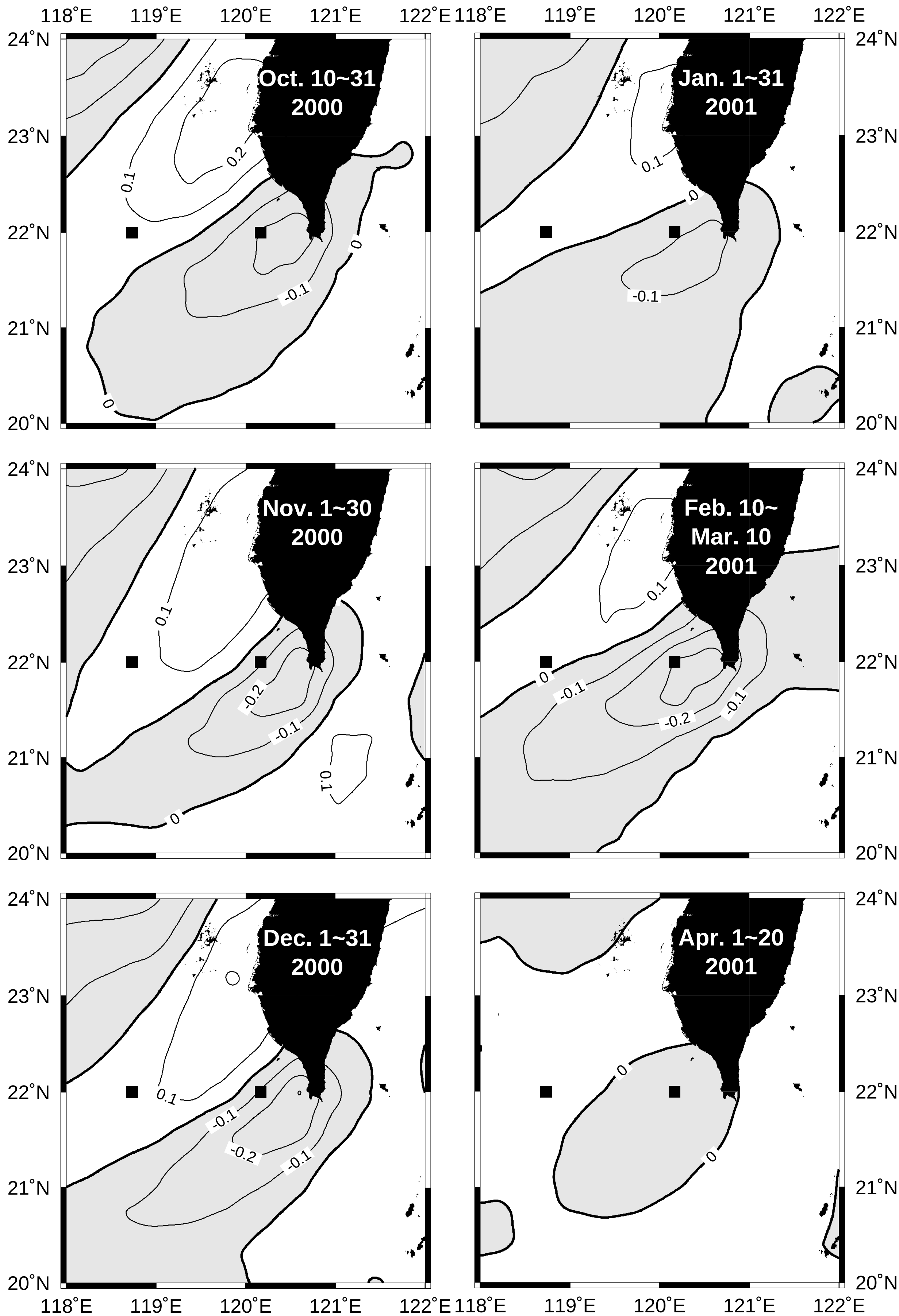

審查者意見

Subject: "Intra-seasonal variation in the velocity field of the northern South China Sea (CSR02)"

I attach two reviews for the afore-mentioned manuscript that you submitted to the special issue of Continental Shelf Research. The first reviewer recommended publication after a minor revision and the second reviewer recommended more convincing interpretations and discussions (see below). Please provide a detailed point-by-point reply to each of the reviewer's comments and either the changes you have made to your manuscript in response to these comments, or rebuttals to the points that you feel are not justified.

On behalf CSR, I thank you for choosing this journal and look forward to seeing your revised manuscript.

Yours sincerely,

Guoqi Han

#1 Review of "Intra-seasonal variation in the velocity field of the northern South China Sea" by Wu et al.

This manuscript uses moored measurements of currents and water properties in the upper ocean at two locations to suggest the possible link between the circulation southwest of Taiwan and the intrusion water from the Kuroshio. Wind stress curls are demonstrated to correlate with the observed current pattern. Although the data duration is not long enough to reach a definitive conclusion, the manuscript does demonstrate an interesting phenomenon in the region southwest of Taiwan, where the interaction of Kuroshio intrusion plays an important role in the circulation, and could help suggest further studies. I would recommend publication of the manuscript. Some minor modifications are listed below.

Page 4, line 5: The data consist of flow velocity and water properties. Thus, the effect of the Kuroshio intrusion can be inferred.

Page 5, 2nd line of section 3.1 "In general, U is greater than V.": Some statistics than just saying it is much better.

Page 5, 2nd line of section 3.1: "The speed decrease ... same direction." Replaced by "The flow is barotropic in the upper 120 m with a slight decrease in magnitude."

Page 5, first paragraph of section 3.1: It is difficult to discuss the current direction using U and V components. It is easier to describe the current using the stick plots Fig. 4. Same for the next paragraph.

Page 8, line 9: The temperature "contrast" is more distinct at W than that at E; the latter location is affected by cold coastal water.

Page 9, last sentence of the first paragraph: The two stations might not be located in the same cyclonic structure.

Page 9, 2nd line from the bottom: deserves "further investigation." Intuitively, currents in "this" area, especially those near "the surface," should ....

Page 10, 5th line: delete "essential."

Page 10, line 9: delete "also."

Page 10, line 12: "are needed" instead of "are indeed in need."

Page 11, line 2: October "2000", a dipole ... with positive "values"

Page 11, line 12: "the southern curl" should be replaced by "the southern pattern" at several places of its occurrence on this and next pages.

#2 Review of "Intra-seasonal variation in the velocity field of the northeastern South China Sea" by C.-R. Wu, T. Y. Tang, S. F. Lin, Y. J. Yang, and W.-D. Liang

This manuscript describes observations from two moorings in the northeastern South China Sea. The moorings were placed in the northern portion of Luzon Strait, just to the west of the strait, and further west over the continental slope. The authors use a combination of mooring data and scatterometer wind stress curl fields to infer characteristics of the Kuroshio Intrusion into the South China Sea.

On the whole, I thought that the mooring data was interesting. For the most part, I thought that the interpretation was sound but could be developed much more convincingly. A few points were contradictory with the existing literature and should be more fully discussed.

The following are major points that should be addressed.

1) How could the wind stress give rise to a 100 cm/s current? Centurioni and Niiler (JPO, 2004) have shown that near surface velocities are well below the observed drifter speeds. What is the mechanism that drives the strong currents? The main reason, I would think, would be the baroclinic currents associated with the density gradients within the Kuroshio, and not the direct action of wind stress. This issue needs to be discussed thoroughly and the drifter work referenced.

2) A simple scaling of the vorticity input from the wind stress curl would be very useful. I am not certain that the wind stress curl is energetic enough to drive a 100 cm/s maximum velocity gyre. A back of the envelope calculation would be useful to convince me that there is enough energy from the wind stress curl to drive the observed anti-cyclonic circulation.

3) I am still confused about the time scale of the intrusions relative to the magnitude of the wind stress curl. It looked to me like there was a great deal of variability in the moorings even when there was strong wind stress curl- and that intrusions were not present. Some figure showing the temporal shift in the wind stress curl magnitude with the anti-cyclonic flow would be useful and again be more convincing.

4) One of the strengths of the paper is showing the high degree of correlation between the E and W moorings. What does this imply for an advection rate? How does the advection rate compare to the propagation speed of a baroclinic Rossby wave?

I thought the work that was presented was very interesting and eventually deserves publication after giving some thought to the issues above. The mooring data was quite interesting, more quantitative treatment of the issues above would greatly help convince the reader of the interpretations.

GEOPHYSICAL RESEARCH LETTERS, VOL. ???, XXXX, DOI:10.1029/,

Energy of Nonlinear Internal Waves in the South China Sea

R.-C. Lien,[1] T. Y. Tang,[2] M. H. Chang,[2] E. A. D'Asaro,[1]

Four sets of ADCP measurements were taken in the South China Sea (SCS); these results were combined with previous satellite observations and internal-tide numerical model results. Analysis suggests that strong internal tides are generated in Luzon Strait, propagate as a narrow tidal beam into the SCS, are amplified by the shoaling continental slope near TungSha Island, become nonlinear, and evolve into high-frequency nonlinear internal waves (NIW). Internal waves in the SCS have geographically distinct characteristics. (1) West of Luzon Strait the total internal-wave energy (E_{iw}) is 10 × that predicted by Garrett and Munk spectra (E_{GM})(Levine, 2002). There is no sign of NIW. (2) Near TungSha Island $E_{iw} = 13 \times E_{GM}$. Strong nonlinear and high-harmonic tides are present. Repetitive trains of large-amplitude NIW appear primarily at a semidiurnal periodicity with their amplitudes modulated at a fortnightly tidal cycle. The rms vertical velocity of NIW shows a clear spring-neap tidal cycle and is linearly proportional to the barotropic tidal height in Luzon Strait with a 1.85-days time lag; this provides an estimate of NIW energy in the SCS. The 1.85-day time lag is consistent with the travel time of internal tides from Luzon Strait to TungSha Island. (3) At the northern SCS shelfbreak, $E_{iw} = 4 \times E_{GM}$. Single depression waves are found, but no multiple-waves packets are evident. (4) On the continental shelf $E_{iw} = 2 \times E_{GM}$. Both depression and elevation NIW exist.

Introduction

Hsu and Liu (2000) and Zhao et al. (2004) collected satellite images between 1993 and 2001 in the SCS to reveal the distribution of NIW (Fig. 1). Most of the long-crest, multiple-wave packets exist in a (200 km)^2 area on the continental slope and shelf centering around TungSha Island. A single long-crest, multiple-wave packet was observed at the west of Luzon Strait on 1995 June 16. In the deep basin of the SCS only a few short-crest wave trains and single-depression waves exist. Recent *in-situ* measurements confirm the presence of NIW identified by satellite images (Ramp et al. 2004 and Yang et al. 2004).

The generation mechanism for NIW in the SCS remains controversial. Two hypotheses have been proposed: the internal soliton/lee wave model, and the nonlinear internal tide model (Fig. 2)(Apel et al., 1997). According to the former, lee waves are generated between the Batan Islands in Luzon Strait. When the current reverses, lee waves escape from the topography and develop into NIW (Fig. 2a). According to the latter, internal tides are generated either on shelf break or remotely on two ridges in Luzon Strait (Fig. 1) (Niwa and Hibiya, 2004). Those generated in Luzon Strait propagate across the SCS in a narrow tidal beam. They are amplified by the shoaling continental slope, become nonlinear, and evolve into NIW riding on the internal tide (Fig. 2b). For very strong barotropic tidal forcing in Luzon Strait, internal tides could be strongly nonlinear near their generation sites so that NIW would evolve immediately (Fig. 2c).

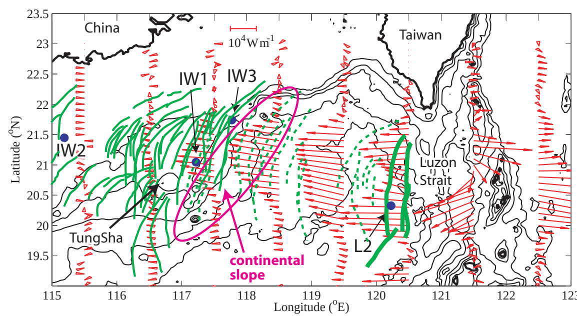

Figure 1. Map of South China Sea and positions of ADCP stations (blue dots). Black contours are 200, 500, 1000, 2000, and 3000-m isobaths. Red vectors are model results of depth-integrated semidiurnal internal tidal energy flux produced by Niwa and Hibiya (2004). Green curves are internal wave packets derived from satellite images by Zhao et al. (2004). Solid green curves indicate multiple-wave packets and dashed green curves single-wave packets. Thick solid green curves west of Luzon Strait represent the "big wave" event observed on 16 June 1995.

Here, we analyze a set of four ADCP measurements taken in different regions of the SCS. We will 1) describe internal wave characteristics, 2) discuss the generation mechanism of NIW, and 3) explore the relation between NIW in the SCS and barotropic tidal forcing in Luzon Strait.

Observations

In April 2000 three 150-kHz broadband ADCP moorings (L2, IW1, and IW3) and one 300-kHz narrowband bottom ADCP (IW2) were deployed in the SCS (Figs. 1 and 2) collecting data for ∼20 days. All ADCPs were upward-looking and recorded 1-min averages. The water depths at stations L2, IW1, IW3, and IW2 were 2080 m, 426 m, 468 m, and 110 m, respectively. The mooring ADCPs were mounted at a nominal depth of 237 m.

Internal Wave Characteristics

Internal waves observed in four locations within the SCS have different characteristics. Segments of 4-hr time series for six consecutive semidiurnal periods illustrate these differences (Fig. 3).

The L2 mooring was located west of a submarine ridge in Luzon Strait. ADCP observations were available between 30 and 220 m depths. The zonal current u dominated the

[1]Applied Physics Lab, University of Washington, Seattle, WA 98105, USA

[2]Institute of Ocean Research, National Taiwan University, Taiwan

0094-8276/04/$5.00

meridional current. We compute the stream function as $\Psi = \int dz(u - C)$, where a wave speed C=1.8 m s^{-1} is used (Yang et al., 2004). The zonal velocity between the sea surface and 30-m depth is assumed constant and equal to $u(30m)$. The computed stream line provides a crude view of the isopycnal displacement. The streamline shows high-frequency variations riding on a low-frequency tidal bore; but no NIW are evident. This is the first *in-situ* evidence confirming the absence of NIW near Luzon Strait. The vertical velocity measurements at L2 were contaminated by instrument noise and are not shown.

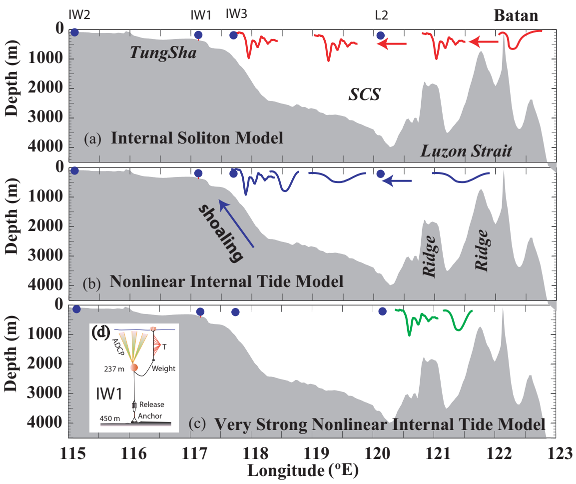

Figure 2. Sketch of generation mechanisms for NIW in the SCS:(a) internal soliton model, (b) nonlinear internal tide model, and (c) very strong nonlinear internal tide model. The shading is the bathymetry across the South China Sea. The inset (d) shows the mooring ADCP configuration. Blue dots indicate locations of ADCP measurements.

At mooring IW1, large NIW were observed at a semidiurnal period. The streamline followed the zonal shear very well, especially within the leading wave. The leading waves had a vertical displacement of 70–120 m, and a wave width of 10–20 minutes corresponding to a 1–2 km-width. These NIW had a first-mode appearance. Before the waves' arrival, the current flowed eastward. During the waves' passage, the zonal current in the upper layer fluctuated in alternating directions. The maximum westward current was $>$ 1 m s^{-1}. The vertical velocity at IW1 showed the unambiguous first-mode depression wave structure, with maximum speed at mid-depth, and downwelling followed by upwelling. The vertical velocity reached 0.2 m s^{-1}. NIW at IW1 were the strongest among our observations, as was expected from satellite images and numerical model results of internal tides (Fig. 1).

At mooring IW3, only single depression waves were observed. The largest depression wave was at 0300 on 21 April. The zonal velocity of the wave was $\sim$0.5 m s^{-1}, less than 1/2 of that observed at IW1. Mooring IW3 was located off shelf relative to the ASIAEX experiment site(Ramp et al., 2004).

Mooring IW2 was located on the continental shelf at $\sim$110-m depth. Two trains of elevation waves were identified at 0300 on 18 April and 0548 on 19 April. A westward wave speed of 0.8 m/s was used to compute the stream function, determined by matching the observed vertical velocity with the prediction from the stream function. The isopycnal displacement was generally $<$10 m. The most distinct characteristic of these elevation waves is the leading upwelling followed by downwelling, best observed for the wave train at 0548 on 19 April.

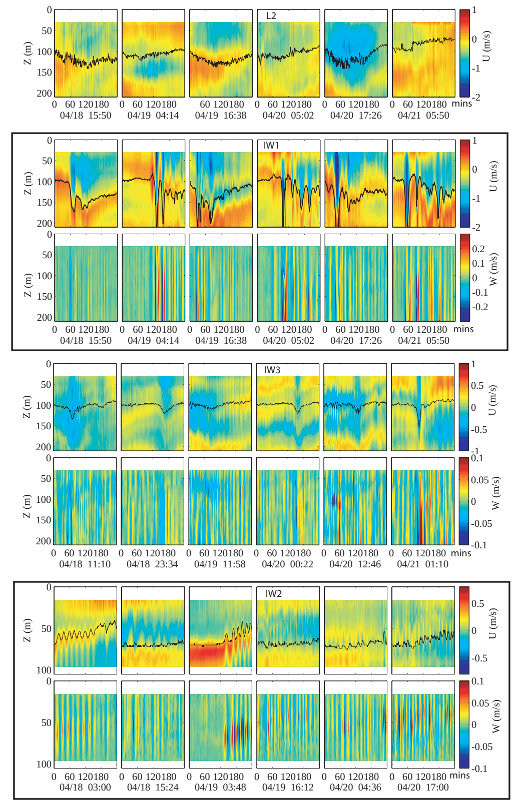

Figure 3. Zonal velocity and vertical velocity contours in 4-hr time segments for six consecutive semidiurnal periods. Each segment is separated by a semidiurnal period 12.4 hr. The vertical velocity at L2 is not shown because it is contaminated by instrument noise. The beginning time for each time segment is shown on the lower line of the x-axis; upper line shows minutes elapsed from the beginning time. The black curve shows the streamline beginning at 100-m depth, assuming a westward wave speed of 1.8 m s^{-1} for L2, IW1, and IW3, and 0.8 m s^{-1} for IW2.

Internal Wave Spectra

Velocity spectra are computed and WKB-normalized at each depth. Spectra are averaged over the upper 100 m and compared with the Garrett–Munk spectra (GM79) (Levine, 2002). The total energy spectrum (Φ_E), horizontal velocity spectrum (Φ_u), vertical velocity spectrum (Φ_w), and potential energy spectrum (Φ_{PE}) of GM79 are expressed as follows,

$$\Phi_E = E_t \frac{N}{N_0} B(\omega) \tag{1}$$

$$\Phi_w = E_t \frac{(\omega^2 - f^2)N}{(N^2 - f^2)N_0} B(\omega) \tag{2}$$

$$\Phi_u = \frac{1}{2} \frac{(N^2 - \omega^2)(\omega^2 + f^2)}{(\omega^2 - f^2)\omega^2} \Phi_w \tag{3}$$

$$\Phi_{PE} = \frac{1}{2}\frac{N^2}{\omega^2}\Phi_w, \quad (4)$$

where $B(\omega) = \frac{2f}{\pi\omega(\omega^2-f^2)^{1/2}}$, ω is frequency, N the buoyancy frequency, and f the inertial frequency. $E_t = 2.9$ mJ kg^{-1} is the total energy per unit mass. $N_0 = 0.0052$ s^{-1} is a reference buoyancy frequency. We compute the potential energy spectrum using the observed vertical velocity spectrum following Eq. (4).

At mooring L2, both horizontal velocity spectra show dominant diurnal and semidiurnal peaks. They have a similar magnitude and show a ω^{-2} spectral shape until they meet the noise floor at about 0.003 s^{-1}. The total internal wave energy E_{iw} is 10 $\times E_{GM}$, where E_{GM} is the total energy of GM79 (Table 1).

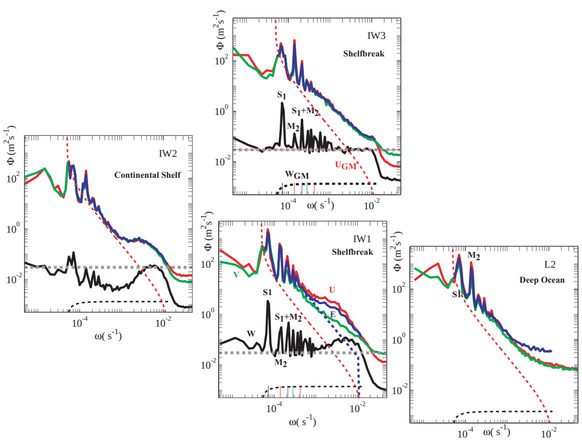

Figure 4. Average velocity and energy spectra. Spectra are WKB-normalized and averaged over the upper 100 m. Red, green, and black curves represent zonal, meridional, and vertical velocity spectra, respectively. Blue curves are total energy spectra. Black and red dashed curves are GM79 vertical and horizontal velocity spectra. The thick dashed gray lines represent the observed vertical velocity spectrum at IW3 averaged in 0.001 s^{-1} $< \omega < N$, plotted for reference. Frequencies of diurnal tide S_1, semidiurnal tide M_2, and the compound tide, $M_2 + S_1$ are labeled. The dashed blue curve in the panel of IW1 represents the background high-frequency internal wave spectrum.

At mooring IW1 observed spectra exhibit peaks at diurnal, semidiurnal, and compound tides, as well as higher tidal harmonics suggesting nonlinear internal tides. At frequencies greater than tidal harmonics, 1) the meridional velocity spectrum Φ_v shows a ω^{-2} shape below N (0.016 s^{-1}), 2) Φ_u shows a plateau of 5 $\times\Phi_v$, and 3) Φ_w shows a bump in 0.001 s^{-1} $< \omega < N$. E_{iw} is 5.76 $\times$ 10^{-2} m^{2}s^{-2}, 13 $\times E_{GM}$ (Table 1). The vertical kinetic energy W^2_{iw} is 0.045 $\times$ 10^{-2} m^{2}s^{-2}, 54 $\times$ the vertical energy of GM (W^2_{GM})! The spectral plateau of Φ_u and the spectral bump of Φ_w below N are associated with the NIW. The strong nonlinear tide and the accompanying enhanced NIW suggest a direct dynamic link, consistent with the nonlinear internal tide model generation mechanism (Fig. 2b).

At mooring IW3 spectral peaks exist at diurnal, semidiurnal, and compound tides, as well as higher tidal harmonic frequencies, similar to IW1 but of weaker magnitudes. Beyond the tidal harmonics, the two horizontal velocity spectra have the same spectral level with a spectral slope slightly greater than -2, and Φ_w is white below N. E_{iw} is 4 $\times E_{GM}$, and W^2_{iw} is 25 $\times W^2_{GM}$. Fundamental differences from IW1 are 1) the absence of the near-N spectral bump of Φ_u and Φ_w at IW3, 2) the total internal wave energy and vertical kinetic energy at IW3 is $<$ 1/2 of those at IW1.

At mooring IW2, all velocity spectra show peaks at the diurnal and semidiurnal frequencies. In 0.001 s^{-1} $< \omega < N$, all spectra exhibit a bump 10 times the background level associated with the mixed elevation and depression NIW (see Fig. 3). E_{iw} is 2 $\times E_{GM}$, and W^2_{iw} is 15 $\times W^2_{GM}$.

The presence of strong NIW at IW1 and their absence at L2 shown in time series and spectral properties suggest that NIW in the SCS are generated via the nonlinear internal tide model (Fig. 2b), not the lee wave model (Fig. 2a).

NIW Energy and Tidal Forcing

NIW contain more than 80% of the vertical energy in the internal wave band (Table 1). Therefore, the vertical energy is an ideal index for NIW energy. The vertical velocity variances at IW1, computed in 1-hr intervals, show a semidiurnal periodicity (Fig. 5b). The barotropic tidal height in Luzon Strait, computed using Oregon Tidal Inversion Software (OTIS) (Egbert and Erofeeva, 2002) is also dominated by the semidiurnal tide (Fig. 5a). Both variables show a fortnightly modulation and are correlated with a 1.85-day phase lag lead by the tide (Fig. 5c). Niwa and Hibiya (2004) show that the M_2 energy flux emanates mostly from the western submarine ridge, 300–350 km from IW1. Considering the 1.85-day phase lag as the travel time, the speed of the semidiurnal internal tide should be 1.88–2.20 m s^{-1}, a reasonable estimate. The correlation between the rms tidal amplitude in Luzon Strait (σ_H) and the rms vertical velocity at IW1 (σ_w) is 0.89 and the linear regression fit (Fig. 5d) yields

$$\sigma_w(m/s) = 0.11\sigma_H(m) - 0.01(m/s). \quad (5)$$

This relation provides a simple model to predict the energy of NIW near TungSha Island based on the barotropic tide at Luzon Strait. The correlation increases to 0.96 and the linear regression fit is improved if the linear trend of σ_w is removed (Fig. 5d).

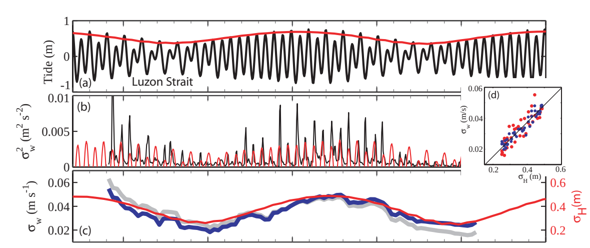

Figure 5. Time series of (a) the barotropic tide east of Luzon Strait H_{LS}((black curve) and the 1.7 $\times$ the rms tidal amplitude computed in 24-hr intervals $\sigma_{H_{LS}}$ (red curve); (b) the vertical velocity variance computed in 1-hr intervals σ^2_w (black curve), and the 1.85-day forward shifted H_{LS} (red curve); (c) the rms vertical velocity σ_w computed in 24-hr intervals (gray curve) and the 1.85-day forward shifted $\sigma_{H_{LS}}$ (red curve). The blue curve in (c) is the detrended σ_w. The inset (d) shows the scatter plot between 1.85-day shifted $\sigma_{H_{LS}}$ and σ_w (red dots), and between 1.85-day shifted $\sigma_{H_{LS}}$ and detrended σ_w (blue dots). The black line represents the linear regression fit.

Discussion and Summary

Generation Mechanisms

Observed internal wave properties combined with a composite map of NIW from satellite images and results of numerical internal tide models supports the hypothesis that the nonlinear internal tide is the primary generation mechanism for NIW observed in the SCS (Fig. 2b). Strong internal tides are generated in Luzon Strait. They propagate into the SCS in a narrow tidal beam (Fig. 1). They are amplified by the shoaling continental slope near TungSha, become nonlinear, and evolve into NIW (Figs. 3 and 4). Observed NIW are not escaping lee waves (Fig. 2a) because they are not observed at L2, contradicting the internal-soliton model. Within the internal tidal beam (e.g., IW1), NIW evolve primarily from the amplification of the trans-basin internal tides. At mooring IW1, the internal wave energy is 13×GM, the vertical energy is 54×GM, and NIW of $O(100m)$ amplitude are observed repeatedly. Outside of the internal tidal beam (e.g., IW3), NIW may evolve from the locally generated internal tides (Ramp et al., 2004).

Big Wave near Luzon Strait

A long-crest NIW was captured by a satellite image on 16 June 1995 (Hus and Liu, 2000). During this event, the barotropic tidal current in Luzon Strait was one of the strongest of 1995 (Fig. 6). The "big wave" west of Luzon Strait may have been generated by an abnormally strong barotropic tidal forcing. These events occur only a few days each year. The chance is small for satellite images to capture these events; only one appears in the satellite record of nearly 10 years.

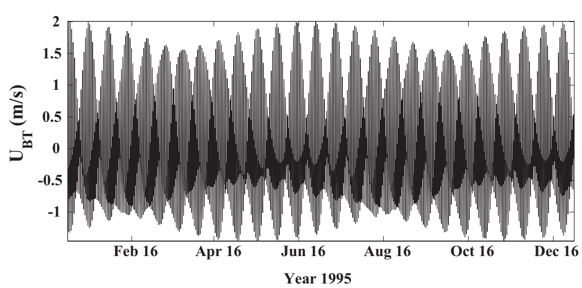

Figure 6. Barotropic zonal tidal current in Luzon Strait in 1995 produced by OTIS (Egbert and Erofeeva, 2002).

Energy Conversion and Dissipation of NIW

At mooring IW1, the total energy in the high-frequency regime (10^{-3} s^{-1} $< \omega < N$) is $\sim$16% of the total internal wave energy (Table 1). The total energy of "non-NIW" high-frequency internal waves is computed by integrating the background internal wave spectrum, constructed by extrapolating a ω^{-2} spectrum from the observed spectral level at 10^{-3} s^{-1} to N (blue dashed curve in Fig. 4). It is $\sim$3% of the total internal wave energy. Therefore, the energy conversion rate from internal tides to NIW is $\sim$13%. Niwa and Hibiya (2004) report an internal tidal energy flux of 4.2 GW into the SCS (Fig. 1). Applying a 13% conversion rate, NIW contain an energy flux of 0.54 GW. If all NIW dissipate within the (200 km)^2 area centered at TungSha Island in the 1–10m-thick interface, the turbulence kinetic energy dissipation rate ε associated with breaking NIW would be $\sim 10^{-6}$–10^{-5} W kg^{-1} and an eddy diffusivity $K_\rho = 0.2\varepsilon N^{-2} =\sim 10^{-3}$–$10^{-2}$ m^2 s^{-1}, at least 100 times that in typical oceanic thermocline.

Prediction of NIW in SCS

The energy content of NIW depends on 1) the conversion rate from the barotropic to internal tides, 2)the conversion rate from internal tides to NIW, 3) the tidal beam properties, and 4) the dissipation of NIW. These processes are modulated by the barotropic tides, by the background shear and stratification associated with Kuroshio, mesoscale eddies, and by the surface wind and buoyancy forcing in the SCS including Luzon Strait. The simple relation (5) includes only one of many important parameters, implying invariant energy conversion rates. The fair success of this simple relation is because other parameters are nearly invariant in a monthly time scale, and at mooring IW1 internal tides generated remotely in Luzon Strait dominates those generated locally. The linear trend of σ_w (Fig. 5c) represents the effects of processes overlooked by Eq. (5). Further observations and numerical models are needed to improve our understanding of the details of these processes, and improve the prediction of NIW.

Acknowledgments. We wish to thank Drs. Yoshihiro Niwa and Toshiyuki Hibiya for providing their model results of internal tidal energy flux in the South China Sea. Discussions with Drs. Wen-Ssn Chuang, Matthew Alford, and Zhongxiang Zhao were very helpful. This work is supported by the Office of Naval Research of US and the National Science Council of Taiwan.

References

Apel, J. R., M. Badiey, C.-S. Chiu, S. Finette, R. Headrick, J. Kemp, J. F. Lynch, A. Newhall, M. H. Orr, B. H. Pasewark, D. Tielbuerger, A. Turgut, K. von der Heydt, and S. Wolf (1997), An overview of the 1995 SWARM Shallow-Water Internal Wave Acoustic Scattering Experiment, *IEEE J. Oceanic Eng.,* , 22, 465–500.

Egbert, G. D. and Erofeeva, S. Y. (2002). Efficient inverse modeling of barotropic ocean tides. *J. Atm. and Ocean. Tech.*, *19*, 183–204.

Hsu, m.-K., and A. K. Liu (2000), Nonlinear internal waves in the South China Sea, *Can. J. Rem. Sens.*, *26*, 72–81.

Levine, M. (2002), A modification of the Garrett-Munk internal wave spectrum, *J. Phys. Oceanogr.*, 32, 3166–3181.

Niwa, Y., and T. Hibiya (2004), Three-dimensional numerical simulation of M_2 internal tides in the East China Sea, *J. Geophys. Res.*, *109*, doi:10.1029/2003JC001923.

Ramp, S. R., D. Tang, T. F. Duda, J. F. Lynch, A. K. Liu, C.-S. Chiu, F. Bahr, H.-R. Kim, and Y. J. Yang (2004), Internal solitons in the northeastern South China Sea Part I:Sources and Deep Water Propagation, *IEEE J. Ocean Eng.*, in press.

Yang, Y. J., T. Y. Tang, M. H. Chuang, A. K. Liu, M.-K. Hsu, and S. R. Ramp (2004), Solitons northeast of TungSha Island during the ASIAEX pilot studies, *IEEE J. Ocean. Eng.*, Special Issue on Asian Marginal Seas, in press.

Zhao, Z., V. Klemas, Q. Zheng, and X.-H. Yan (2004), Remote sensing evidence for baroclinic tide origin of internal solitary waves in the northeastern South China Sea, *Geophys. Res. Let.*, *31*, doi:10.1029/2003GL019077.

R.-C. Lien, Applied Physics Lab, University of Washington, Seattle, WA 98105, USA. (lien@apl.washington.edu)

Table 1. Characterization of energy measurements at four stations in the SCS averaged in the upper 100 m: W_{iw}^2, vertical kinetic energy in the internal wave band; E_{iw}, total internal wave energy; $\frac{W_{iw}^2}{W_{GM}^2}$, the ratio of W_{iw}^2 to the GM79 vertical kinetic energy W_{GM}^2; $\frac{E_{iw}}{E_{GM}}$, the ratio of E_{iw} to GM total energy E_{GM}; W_{NIW}^2, the vertical kinetic energy in the high-frequency regime ($10^{-3}\text{s}^{-1} < \omega < N$); E_{NIW}, the total energy in the high-frequency regime; $\%W_{NIW}^2$, the percentage of W_{NIW}^2 in W_{iw}^2; and $\%E_{NIW}$, the percentage of E_{NIW} in E_{iw}.

Stn	W_{iw}^2 ($\frac{cm^2}{s^2}$)	E_{iw} ($\frac{cm^2}{s^2}$)	$\frac{W_{iw}^2}{W_{GM}^2}$	$\frac{E_{iw}}{E_{GM}}$	W_{NIW}^2 ($\frac{cm^2}{s^2}$)	E_{NIW} ($\frac{cm^2}{s^2}$)	$\%W_{NIW}^2$ (%)	$\%E_{NIW}$ (%)
L2	NA	546	NA	10.2	NA	NA	NA	10
IW1	4.5	576	53.5	12.9	4	92	89	16
IW3	2.1	243	24.8	4.3	1.7	26	81	11
IW2	1.3	140	14.7	2.4	1.2	20	93	14

3. 討論

在“Intra-seasonal variation in the velocity field of the northeastern South China Sea”一文中，我們討論分析該處量測的海流變化，並推論其與 wind stress curl 之關係。然近期亦有結果顯示，eddy shelding、double eddies 存在等因子，也可能造成此區流場呈季節內變化。進一步藉助數值模式分析仍在進行中。

而在”Energy and Characteristics of Nonlinear Internal Waves in South China Sea”一文中分析北南海陸棚錨碇海流資料，顯示當地的 Internal Soliton Wave 源自於呂宋海峽由半日潮產生及 local generation。然對於其他的動力機制(如全日潮等)則須進一步分析。